Calculation of screened Coulomb potential matrices and its application to He bound and resonant states

Li Guang Jiao* and Yew Kam Ho†

Institute of Atomic and Molecular Sciences, Academia Sinica, P.O. Box 23-166, Taipei 106, Taiwan

(Received 8 May 2014; published 21 July 2014)

We present two analytical methods, Taylor expansion and Gegenbauer expansion, to efficiently and accurately calculate the two-electron screened Coulomb potential matrix elements with Slater-type configuration-interaction basis functions. The former permits great advantages in fast computation of the potential matrices at small screening parameters and the latter allows accurate calculation of the matrices at all screening parameters. The bound and resonant states of a He atom embedded in the screening environment are calculated by employing the variational and complex-scaling methods, respectively, and the results are compared with other theoretical predictions. The expectation values of some physical quantities for He ground state are compared with the recent calculation of Ancarani and Rodriguez [Phys. Rev. A **89**, 012507 (2014)] and extended to stronger screening environment. The energies and widths for the doubly excited resonant states are in good agreement with previous calculations, while the interelectronic angle $\arccos\langle\cos(\theta_{12})\rangle$ show significant discrepancies with the Feshbach projection calculation of Ordóñez-Lasso *et al.* [Phys. Rev. A **88**, 012702 (2013)]. The expectation values of $\langle \mathbf{p_1}\cdot\mathbf{p_2}\rangle$ are also calculated for the resonant states investigated here. We conclude that the present methods in the framework of complex scaling enable us to get reliable energy, width, and other physical quantities of the resonant states in a variety of screening conditions.

DOI: 10.1103/PhysRevA.90.012521 PACS number(s): 31.15.ve, 31.15.vj, 32.80.Zb

I. INTRODUCTION

Investigation of the screened Coulomb potential (SCP) has attracted considerable attention in the past years due to its fundamental importance and wide applications in different areas, such as atomic physics, nuclear physics, plasma physics, semiconductors, and quantum chemistry [1–15]. In a variety of formalism, the exponential type in the form $Z_iZ_je^{-\lambda r_{ij}}/r_{ij}$ with λ the screening parameter is of particular interest. For example, it can be used to describe the Coulomb interactions of atoms embedded in weakly coupled plasmas within the Debye-Hückel model where the screening parameter is a function of plasma temperature and number density of charged particles [1–7], the interactions of elementary particles in nuclear structure calculations where the SCP is always referred to as Yukawa potential [8,9], and the static field generated by impurity doping in semiconductor materials where the screening parameter is related to the impurity charge and electron and impurity concentrations [10,11]. The SCP has also shown its special advantages in implementation of the range-separated density-functional theory [12,13]. With the recent advances [14,15] in employing the Slater-type orbitals as the basis sets in the quantum chemistry calculations, the exponential function $e^{-\lambda r_{ij}}$, which in combination with the r_{ij}^{-1} factor gives the exponential-type SCP, appears as a natural choice of the complementary error function in the range-separated density-functional theory.

Earlier interests of SCP in atomic systems are mostly related to the one-electron problems for which the energies and transitions of the ground and excited states have been investigated extensively by many authors [16–20]. The screening effects of SCP on the two-electron bound systems have also been performed in the framework of variational method by authors employing different types of basis sets, such as the product of a hydrogenlike basis [21], the Slater-type configuration-interaction (CI) basis [22,23], the Hylleraas basis [24–27], the exponential correlated basis [28–30], and the B-spline CI basis [31,32]. Bound energies of the ground, singly excited, and some doubly excited metastable bound states for the two-electron atoms or exotic three-body systems have been calculated with very high accuracy. Most recently, Ancarani and Rodriguez [33] have investigated the evolution of radial expectation values for the ground state of H^-, He, and Li^+ atoms with respect to the screening parameter by using a C3-like basis. Such investigations on physical quantities other than bound energy are of special interest in furthering our understandings about the system structure and dynamics in a screening environment. However, their calculations are restricted to relatively weak screening conditions and the accuracy of their results is somewhat limited. Alternative investigations on this problem are warranted.

Recent theoretical interests for atoms interacting with SCPs have been concentrated on the autoionizing resonant states due to their important roles in the processes of photoionization, electron-atom scattering, laser-atom interaction, etc. Several powerful methods originally developed for atoms in pure Coulomb interactions have been extended to the screening situation. For example, those methods based on scattering mechanism extract the resonance parameters by calculating the cross sections, phase shifts, or eigenphase sums and fitting them with the Breit-Wigner formula, such as the close-coupling method [34,35] and the R-matrix method with pseudostates [36,37]. Other widely used methods calculate the resonances in more "direct" ways, in either the real or the complex energy plane, by using the bound-state (L^2)-type

*guang5678@gmail.com
†ykho@pub.iams.sinica.edu.tw

wave functions, such as the stabilization method [38–40] and the complex-scaling method [41–43]. Although a considerable number of efforts have been made throughout years on a variety of atomic targets [34–43], most of these works were focused on the resonance energy and width. The studies on other physical properties of resonant states are very scarce. Ordóñez-Lasso *et al.* [44] have recently made a comprehensive investigation on the energy, width, and average interelectronic angle [calculated by $\arccos\langle\cos(\theta_{12})\rangle$] for the resonant states lying below the $He^+(N=2)$ threshold by using the Feshbach projection method with Hylleraas basis functions. It has been shown that, in some circumstances, the evolution of average interelectronic angle against the screening parameter is very complicated, while the variations of resonance energy and width are generally in regular ways. It is known that the quantity $\langle\cos(\theta_{12})\rangle$ is important in classifying the two-electron resonances into different series labeled by approximate quantum numbers ${}_N[K,T]_n$ [45,46]. The investigation on such quantity would provide more information on the classification of resonant states in screening environment. Moreover, the stabilization and the Feshbach projection methods adopted by previous authors are more applicable in investigating the resonances lying below the first autoionization threshold. For resonances associated with higher-lying thresholds, investigations on their expectation values for physical quantities in relation to the radial, angular, and momentum correlations are still not available in the literature. Such work is very interested in revealing the isomorphic patterns between resonances associated with different thresholds.

In this work, we employ the complex-scaling method [47–49] to investigate the variation of resonant states for a He atom embedded in screening environment. The evolutions of resonance energy, width, and other important physical quantities against the screening parameter are demonstrated in detail. The CI basis functions constructed by the products of one-electron Slater-type orbitals are used to expand the system wave functions. Although it is well known that such a nonexplicitly correlated basis does not fulfill the Kato cusp condition [50] at the two-electron coalescence, reasonably good energies for the lower-lying bound and resonant states can be obtained by using suitably chosen, large numbers of basis functions. On the other hand, for the higher-lying states where the two electrons populate areas far away from each other, the contribution of electron correlations is relatively small and the CI basis would get accurate results comparable to those by the explicitly correlated basis.

The paper is organized as follows. In Sec. II, we present two methods to analytically deal with the two-electron SCP matrices with CI basis functions. They are then applied into the variational and complex-scaling methods to calculate the bound and resonant states, respectively. In Sec. III, the He bound states $1snl$ for $n \leqslant 6$ and the doubly excited resonant states associated with the He^+ ($N = 2$, 3, and 4) thresholds in ${}^1S^e$ and ${}^1P^o$ configurations are calculated. Comparisons with other theoretical predictions are made with special emphasis on the variations of expectation values of the interelectronic angle and momentum quantity. Section IV gives a summary of present work and some future applications of the present method. Atomic units are used unless otherwise noted.

II. THEORY

The nonrelativistic Hamiltonian of a two-electron system interacting with SCPs is given by

$$H = -\frac{1}{2\mu}\nabla_1^2 - \frac{1}{2\mu}\nabla_2^2 - \frac{1}{M}\nabla_1\cdot\nabla_2 - Z\frac{e^{-\lambda r_1}}{r_1} - Z\frac{e^{-\lambda r_2}}{r_2} + \frac{e^{-\lambda r_{12}}}{r_{12}}, \tag{1}$$

where r_1 and r_2 are the radial coordinates of the two electrons from the nucleus with positive charge Z and mass M, and r_{12} is the relative distance between the two electrons. $\mu = mM/(m+M)$ is the reduced mass of the electron with respect to the nucleus. The screening parameter λ is defined by $\lambda = 1/D$, where D is often referred to as Debye length in weakly coupled plasmas.

The following CI basis functions are used to represent the two-electron system wave functions:

$$\Psi(r_1,r_2) = (1-\hat{P}_{12})\sum_{l_a,l_b}\sum_{i,j} C_{a_i,b_j}\eta_{a_i}(r_1)\eta_{b_j}(r_2) \times Y^{LM}_{l_a,l_b}(\hat{r}_1,\hat{r}_2)S(\sigma_1,\sigma_2). \tag{2}$$

η is the radial part of the one-electron Slater orbital,

$$\eta_{a_i}(r) = r^{n_{a_i}-1}e^{-\alpha\xi_{a_i}r}, \tag{3}$$

in which α is a nonlinear scaling parameter to be determined in the calculation. η will be suitably chosen depending on the problem investigated. Y and S are the two-electron total angular momentum and spin-wave functions, respectively. Although the wave functions of Eq. (2) may not produce highly accurate results as the correlated ones, it deserves to be considered due to several advantages: (a) The kinetic energy operators can be easily handled without expanding them on the nonindependent coordinates; (b) the calculation of the expectation values of some physical quantities through CI wave functions is more direct; (c) the CI wave functions are more easy to extend to multielectron systems than the correlated ones which makes further applications of the computational techniques presented here.

The evaluations of the one-electron kinetic and potential matrix elements have no difficulties, while accurate treatment of the two-electron potential part,

$$V_{12}(\lambda) = \langle i,j|\frac{e^{-\lambda r_{12}}}{r_{12}}|k,l\rangle, \tag{4}$$

is more involved. In addition, to calculate the resonant states in the complex-scaling method where all the radial coordinates in the Hamiltonian are rotated by an angle θ,

$$r_{ij} \to r_{ij}e^{i\theta}, \tag{5}$$

one has to deal with the complex potential matrices,

$$V_{12}(\lambda,\theta) = \langle i,j|\frac{\exp(-\lambda r_{12}e^{i\theta})}{r_{12}e^{i\theta}}|k,l\rangle. \tag{6}$$

By making the substitution

$$\lambda' = \lambda e^{i\theta}, \tag{7}$$

Eq. (6) transforms to

$$V_{12}(\lambda',\theta) = \langle i,j|\frac{e^{-\lambda' r_{12}}}{r_{12}}|k,l\rangle e^{-i\theta}, \tag{8}$$

where λ' is a complex screening parameter. Equation (4) can be considered as a special case of Eq. (8) at $\theta = 0$. Many methods based on expansion techniques have been promoted to calculate the above equation, such as the Legendre expansion, series expansion, and the Gegenbauer expansion of the SCP [51,52]. However, these methods contain either a numerical quadrature algorithm or special functions must be calculated numerically. Furthermore, the feasibility of applying these method into complex-scaling formalism still needs further consideration. In the following work, we introduce two analytical methods and demonstrate how to efficiently and accurately calculate the complex-scaled two-electron SCP matrices.

A. Taylor expansion

A direct method to expand the two-electron SCP is through the Taylor expansion,

$$\frac{\exp(-\lambda r_{12}e^{i\theta})}{r_{12}e^{i\theta}} = \sum_{n=0}^{n_{\max}}(-1)^n\frac{\lambda^n}{n!}r_{12}^{n-1}e^{i(n-1)\theta}. \tag{9}$$

The infinite summation over n is truncated at $n_{\max}$ due to computational limitation. The Taylor series is expected to be converged for screening parameters $\lambda < 1$, provided the number of expansion terms is large enough. In our previous work [42], we have tentatively applied this method to calculate the He resonances with SCPs but employing a linear approximation ($r_{12} \approx r_1 + r_2$) for the r_{12} coordinate. Admittedly, such an approximation would lead to unreliable results for the resonances in a strong screening environment. To perform an exact calculation of the r_{12}^{n-1} factors, we use the multipole expansion given by Perkins [53],

$$r_{12}^{\nu} = \sum_{q=0}^{L_1} P_q(\cos\theta_{12})\sum_{k=0}^{L_2} C_{\nu,q,k}\, r_<^{q+2k}\, r_>^{\nu-q-2k}, \tag{10}$$

where, for even values of ν, $L_1 = \frac{1}{2}\nu$ and $L_2 = \frac{1}{2}\nu - q$, and for odd values of ν, $L_1 = \infty$ and $L_2 = \frac{1}{2}(\nu+1)$. $r_<$ and $r_>$ are the smaller and larger of r_1 and r_2, respectively. $P_q(\cos\theta_{12})$ is the Legendre polynomial

$$P_q(\cos\theta_{12}) = \frac{4\pi}{2q+1}\sum_{m=-q}^{q} Y_{q,m}^*(\hat{r_1})Y_{q,m}(\hat{r_2}), \tag{11}$$

and the coefficient $C_{\nu,q,k}$ has the following expression:

$$C_{\nu,q,k} = \frac{(2q+1)}{(\nu+2)}\frac{(\nu+2)!}{(2k+1)!(\nu-2k+1)!} \times \prod_{t=0}^{\min\{(q-1),[(\nu+1)/2]\}}\frac{(2k+2t-\nu)}{(2k+2q-2t+1)}. \tag{12}$$

The r_{12}^{n-1} coordinates are decomposed into $r_<$ and $r_>$ and, therefore, all the integrals can be calculated analytically. The Taylor expansion has special advantages in fast performing the complex-scaling calculations due to the separation of the radial coordinate r_{12} (or $r_<$ and $r_>$) with the screening parameter λ and rotation angle θ. One only needs to calculate the matrix elements of $\langle i,j|r_{12}^{n-1}|k,l\rangle$ one time by using Eq. (10) for all values of n needed; the data can be used repeatedly for arbitrary rotational angles in various screening conditions of $\lambda < 1$. The only price to pay is that the convergence of the Taylor series should be examined carefully.

B. Gegenbauer expansion

Due to the major restriction of the Taylor expansion method, the screening parameter cannot be very large where the Taylor expansion is cumbersome or has even failed; an alternative method by using Gegenbauer expansion [54] has been proven to be effective. The two-electron SCP is expanded by

$$\frac{e^{-\lambda r_{12}}}{r_{12}} = \sum_{L=0}^{\infty}(2L+1)\frac{I_{L+\frac{1}{2}}(\lambda r_<)}{(r_<)^{\frac{1}{2}}}\frac{K_{L+\frac{1}{2}}(\lambda r_>)}{(r_>)^{\frac{1}{2}}}P_L(\cos\theta_{12}), \tag{13}$$

where $I(z)$ and $K(z)$ are modified Bessel functions of the first and second kinds, respectively. The parameter λ can be any complex values. Previous investigations [32,36,37,52] based on such expansion relied on numerical computations of the Bessel functions as well as the two-dimensional integration. Under some circumstances, accurate calculation of the Bessel function itself with complex variables might become very difficult. An analytical treatment turns out to be helpful.

The Gegenbauer expansion reproduces (at $\lambda = 0$) the Laplace expansion of the pure Coulomb potential,

$$\frac{1}{r_{12}} = \sum_{L=0}^{\infty}\frac{(r_<)^L}{(r_<)^{L+1}}P_L(\cos\theta_{12}). \tag{14}$$

Therefore, the general process to calculate the two-electron pure Coulomb potential matrices can be extended to the screened situation. The integration of Eq. (4) is separated into radial and angular parts, and the radial part has the form

$$R^{L+\frac{1}{2}}(i,j,k,l) = \int_0^\infty dr_1\int_0^\infty dr_2(2L+1)r_1^2r_2^2 \times \eta_i(r_1)\eta_j(r_2)\eta_k(r_1)\eta_l(r_2) \times \frac{I_{L+\frac{1}{2}}(\lambda r_<)}{(r_<)^{\frac{1}{2}}}\frac{K_{L+\frac{1}{2}}(\lambda r_>)}{(r_>)^{\frac{1}{2}}}. \tag{15}$$

We then split the two-dimension integration into two ranges,

$$R^{L+\frac{1}{2}}(i,j,k,l) = (2L+1)R_\triangle^{L+\frac{1}{2}}(i,j,k,l) + (2L+1)R_\triangle^{L+\frac{1}{2}}(j,i,l,k), \tag{16}$$

where in the range $r_1 \leqslant r_2$ it has

$$R_\triangle^{L+\frac{1}{2}}(i,j,k,l) = \int_0^\infty dr_1 r_1^{(n_i+n_k-\frac{1}{2})}e^{-(\xi_i+\xi_k)r_1}I_{L+\frac{1}{2}}(\lambda r_1) \times \int_{r_1}^\infty dr_2 r_2^{(n_j+n_l-\frac{1}{2})}e^{-(\xi_j+\xi_l)r_2}K_{L+\frac{1}{2}}(\lambda r_2). \tag{17}$$

The following procedure concerns finding the solution of Eq. (17). After the pioneering work of Seth and Ziegler [14], the exact expression of this integral has been derived by Rico

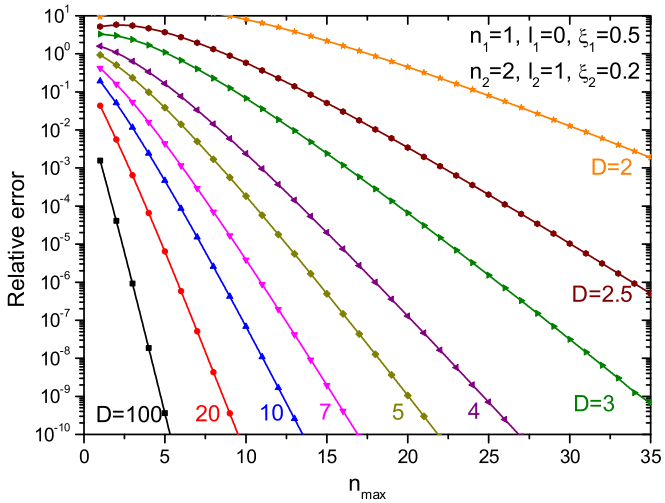

FIG. 1. (Color online) Relative error of Taylor expansion in calculating Eq. (18) with respect to the expansion number $n_{\max}$ at different Debye length D.

et al. [15]. However, the derivation processes of these authors are quite complicated and not easily followed. There are also some typos in their formalism. In the Appendix, we present a much easier process to reproduce the final expression.

C. Convergence

Although from Eq. (9) it can be roughly estimated that the error of the potential by using Taylor expansion truncated at $n_{\max}$ is about $\lambda^{n_{\max}+1}$, it is necessary to quantitatively estimate the convergence of the matrix elements at different screening parameters. We have calculated the matrices,

$$V_{12}(\lambda) = \langle (1s,2p)^1P^o | \frac{e^{-\lambda r_{12}}}{r_{12}} | (1s,2p)^1P^o \rangle, \tag{18}$$

for Debye length D at 100, 20, 10, 7, 5, 4, 3, 2.5, and 2 a.u. by using $n_{\max}$ from 1 to 35. The relative error to the "exact" results calculated by employing Gegenbauer expansion method is defined by

$$\varepsilon = \left| \frac{V_{\text{Taylor}} - V_{\text{Gegenbauer}}}{V_{\text{Gegenbauer}}} \right|. \tag{19}$$

All the results are displayed in Fig. 1 and some numerical values at $D = 10$ are shown in Table I.

It can be seen that the Taylor series exponentially converge to the "exact" value with increasing the expansion number. The relative error of the matrix elements is slightly larger than that for the potential operator itself. We can generally conclude that, for $D \geqslant 10$, the use of $n_{\max} = 15$ in Taylor expansion is sufficiently large to get the matrix elements with more than 10 significant digits.

D. Complex-scaling method

For atomic bound states, the Rayleigh-Ritz variational method is applicable to find the local minimum of the system energy with respect to the variational parameter α shown in Eq. (3). For the resonant states where their wave functions diverge in the asymptotic region, the employing of the complex-scaling method [47–49] is convenient to predict the resonance energy and width. Expectation values of physical quantities can also be calculated through the complex-scaled resonance wave function. A brief review of this method is given here.

TABLE I. Convergence of the Taylor expansion at $D = 10$. "Exact" refers to the result calculated by using the Gegenbauer expansion. $a(b)$ represents $a \times 10^{-b}$.

$n_{\max}$	V	ε
0	0.205 829 770 475 454	5.7136(−01)
1	0.105 829 770 475 454	1.9207(−01)
2	0.137 652 027 002 609	5.0872(−02)
3	0.129 460 363 548 303	1.1665(−02)
4	0.131 305 946 154 959	2.4245(−03)
5	0.130 926 910 857 889	4.6914(−04)
6	0.130 999 624 447 825	8.5976(−05)
7	0.130 986 384 692 241	1.5099(−05)
8	0.130 988 698 208 708	2.5626(−06)
9	0.130 988 307 144 906	4.2289(−07)
10	0.130 988 371 468 016	6.8174(−08)
11	0.130 988 361 126 646	1.0775(−08)
12	0.130 988 362 757 411	1.6745(−09)
13	0.130 988 362 504 481	2.5644(−10)
14	0.130 988 362 543 150	3.8774(−11)
15	0.130 988 362 537 312	5.7942(−12)
16	0.130 988 362 538 184	8.6262(−13)
Exact	0.130 988 362 538 071	

After the rotation of radial coordinates by using Eq. (5), the Hamiltonian is transformed into complex energy plane. The eigenvalues and eigenvectors of the system are calculated by solving the generalized eigenvalue problem at different scaling parameter α and rotational angle θ. The resonance poles are determined by finding the positions where the complex eigenvalues exhibit the most stabilized characters with respect to the changes of both α and θ,

$$\left. \frac{|\partial E_{\text{res}}|}{\partial \theta} \right|_{\alpha=\alpha_{\text{opt}}} = \min, \quad \left. \frac{|\partial E_{\text{res}}|}{\partial \alpha} \right|_{\theta=\theta_{\text{opt}}} = \min. \tag{20}$$

Once the position of a resonance is determined at α_{opt} and θ_{opt} in the complex energy plane, the resonance energy (E_r) and total width (Γ) are given by

$$E_{\text{res}} = E_r - \tfrac{1}{2} i \Gamma. \tag{21}$$

In the complex-scaling method, the divergent outgoing wave function for a resonant state becomes square integrable after rotating the interparticle coordinates. The corresponding incoming wave should be used as its adjoint state,

$$\langle \Psi(-\theta)| = \langle \Psi(\theta)^*|. \tag{22}$$

This is necessary since $H(\theta)$ is no longer self-adjoint; i.e., if $|\Psi(\theta)\rangle$ is a right eigenvector of $H(\theta)$ with eigenvalue E_{res}, $\langle \Psi(-\theta)|$ is the left eigenvector corresponding to the same eigenvalue [55,56]. After the normalization of the resonance wave function

$$\langle \Psi_j(-\theta) | \Psi_i(\theta) \rangle = \delta_{ij}, \tag{23}$$

we can calculate the expectation value of the operator $\hat{O}$ for a single resonance,

$$\langle \hat{O} \rangle_i = \langle \Psi_i(-\theta) | \hat{O}(\theta) | \Psi_i(\theta) \rangle, \tag{24}$$

such as $\langle r_1^n \rangle$, $\langle r_{12}^n \rangle$, $\langle r_< \rangle$, $\langle r_< \rangle$, $\langle T \rangle$, $\langle V \rangle$, $\langle \mathbf{r_1} \cdot \mathbf{r_2} \rangle$, $\langle \mathbf{p_1} \cdot \mathbf{p_2} \rangle$, and $\langle \cos(\theta_{12}) \rangle$. Due to the fact that $\cos(\theta_{12})$ is irrelevant to the radial coordinates, there is no rotation on it. $\langle r_{12}^n \rangle$ can be calculated through Eq. (10), and $\langle \mathbf{r_1} \cdot \mathbf{r_2} \rangle$ and $\langle \mathbf{p_1} \cdot \mathbf{p_2} \rangle$ can be followed from Ref. [57]. It should be kept in mind that the expectation values of these quantities for resonant states are always complex. For the Hamiltonian itself, the imaginary part is half of the decay width Γ [see Eq. (21)] and it can be interpreted as the uncertainty of the energy observable due to decay of the resonance. In such sense, the imaginary part of the expectation value for these physical quantities describes an additional broadening of the distribution of the corresponding observable which is an intrinsic requirement of quantum mechanical uncertainty [56].

III. RESULTS AND DISCUSSIONS

A. Bound states

In this section, we investigate the screening effect of SCP on the bound states of a He atom with infinite nuclear mass ($M = \infty$). The CI basis is constructed by using three groups of Slater orbitals defined in Eq. (3): The first group contains 10 s-, 10 p-, 9 d-, 8 f-, 7 g-, 6 h-, 5 i-, 4 k-, 3 l-, 2 m-, and 1 n-type Slater orbitals with all $\xi = 1.0$, the second one contains 5 s-, 5 p-, 4 d-, 3 f-, 2 g-, and 1 h-type orbitals with $\xi = 0.4$, and the third one has 3 s-, 3 p-, 2 d-, and 1 f-type orbitals with $\xi = 0.2$. These three groups would couple to a total of 648 and 1020 terms in the expansion of system wave functions in $^1S^e$ and $^1P^o$ symmetries, respectively. Such a basis set corresponds to an extensive representation of the system wave function in both the close- and far-range space sectors. To estimate the quality of this basis set, we have calculated the energies of the ground and lowest five excited states for He atom in pure Coulomb interactions where highly accurate results are available. From Table II it can be seen that our results generally have six significant digits in agreement as compared with the Hylleraas calculations of Yan and Drake [59,61], except for the ground state, where our result is about 0.000 04 a.u. higher. This is not surprising due to the strong correlations of the two electrons in the same shell. The results would improve further if optimized ξ values are used in each group. We have also compared our results with the recent B-spline CI calculations of Lin *et al.* [32,58] using an almost 4000 basis. It is found that the present results are even better for the ground state.

The variations of bound-state energies for He atom in screening environment have already been investigated by authors employing different types of basis, such as the three-parameter correlated wave function of Lam and Varshni [21], the Hylleraas basis of Dai *et al.* [24] and Hashino *et al.* [26], the 15-parameter correlated wave function based on Slater orbitals of Saha *et al.* [25], the exponential correlated basis of Kar and Ho [29,30], the B-spline CI basis of Lin *et al.* [32], and the parameter-free C3-like basis of Ancarani and Rodriguez [33]. The present calculations are performed by using the CI basis introduced above and utilizing the methods presented in Sec. II. The results at $\infty \leqslant D \leqslant 20$ are calculated by Taylor expansion with $n_{\max} = 15$ and they show no differences from those obtained by Gegenbauer expansion for practical purpose. A comprehensive comparison between these predictions is illustrated in Fig. 2 and the ground-state energies are shown in Table III for some selected values of D. In the relatively strong screening environment ($\lambda > 1$), our results agree very well with the calculations of Kar and Ho [29] and Lin *et al.* [32], while the results of Lam and Varshni [21] and Saha [25] would exceed the $He^+(1s)$ threshold at $\lambda = 2$. Taking a detailed look at Table III, it is interesting to find that our results show systematically higher energies (0.000 04 a.u. as in the pure Coulomb situation) than the most accurate results of Kar and Ho [29], except at $\lambda \geqslant 2$, where our results are converged to lower energies. Another striking aspect is that the present calculations employing a much smaller number of basis are close to or slightly better than the B-spline CI calculations of Lin *et al.* [32]. The diffuse character of Slater orbitals, multiple groups of basis functions, and accurate computation of matrix elements in analytical expressions are probably responsible for such result. Previous investigations on the singly excited states are very limited. In Fig. 2(b) we compare our results mainly with the B-spline CI calculation of Lin *et al.* [58]. The agreement is generally within the same accuracy as those shown in Table II at $\lambda = 0$.

The investigation on the evolution of physical quantities of He ground state is motivated by the work of Ancarani and Rodriguez [33]. Their investigations are restricted to the radial quantities and in a relatively weak screening environment ($\lambda \leqslant 1.2$). In this work, we present a detailed research on the

TABLE II. Energies and $\langle \cos(\theta_{12}) \rangle$ for the He ground and the lowest five singly excited state in $^1S^e$ and $^1P^o$ symmetries. All results are given in atomic units.

$^1S^e$	E	$\langle \cos(\theta_{12}) \rangle$	$^1P^o$	E	$\langle \cos(\theta_{12}) \rangle$
$1s^2$	−2.903 683	−0.064 22			
	−2.903 582[a]	−0.064 27[a]			
	−2.903 724 3[b]	−0.064 59[c]			
$1s2s$	−2.145 964	−0.014 66	$1s2p$	−2.123 839	−0.004 78
	−2.145 965[a]	−0.014 66[a]		−2.123 832[a]	−0.004 79[a]
	−2.145 974 0[b]	−0.014 70[c]		−2.123 843 0[d]	−0.004 88[c]
$1s3s$	−2.061 265	−0.004 32	$1s3p$	−2.055 144	−0.001 18
	−2.061 269[a]	−0.004 32[a]		−2.055 143[a]	−0.001 18[a]
	−2.061 271 9[b]	−0.004 33[c]		−2.055 146 3[d]	−0.001 25[c]
$1s4s$	−2.033 581	−0.001 80	$1s4p$	−2.031 067	−0.000 47
	−2.033 585[a]	−0.001 80[a]		−2.031 068[a]	−0.000 47[a]
	−2.033 586 7[b]	−0.001 80[c]		−2.031 069 6[d]	−0.000 47[c]
$1s5s$	−2.021 172	−0.000 91	$1s5p$	−2.019 904	−0.000 23
	−2.021 176[a]	−0.000 91[a]		−2.019 905[a]	−0.000 23[a]
	−2.021 176 8[b]	−0.000 91[c]		−2.019 905 9[d]	−0.000 23[c]
$1s6s$	−2.014 558	−0.000 52	$1s6p$	−2.013 831	−0.000 13
	−2.014 563[a]	−0.000 52[a]		−2.013 833[a]	−0.000 13[a]
	−2.014 563 0[b]	−0.000 52[c]		−2.013 833 9[d]	−0.000 13[c]

[a]Lin *et al.* [32,58].
[b]Drake and Yan [59].
[c]Koga *et al.* [60].
[d]Drake and Yan [61].

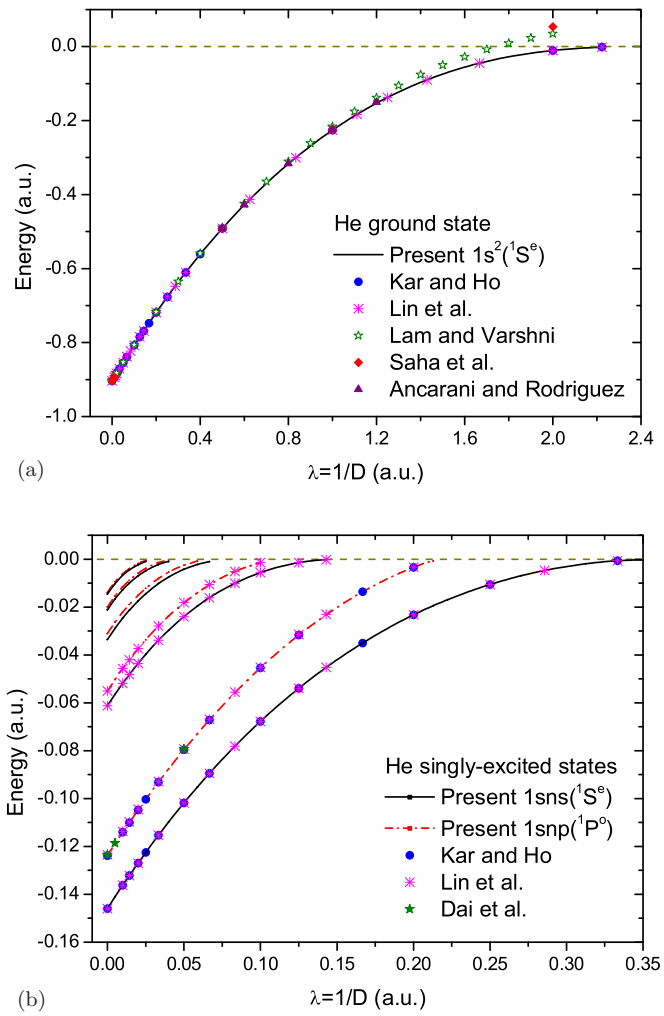

FIG. 2. (Color online) Variation of the He bound-state energies ($\Delta E = E_{\mathrm{He}} - E_{\mathrm{He}^+(1s)}$) against the screening parameter λ. (a) Ground state; (b) singly excited states, where $n = 2$–5 represent lines from bottom to top. Present results are compared with the calculations of Kar and Ho [29], Lin *et al.* [32], Lam and Varshni [21], Saha *et al.* [25], Ancarani and Rodriguez [33], and Dai *et al.* [24].

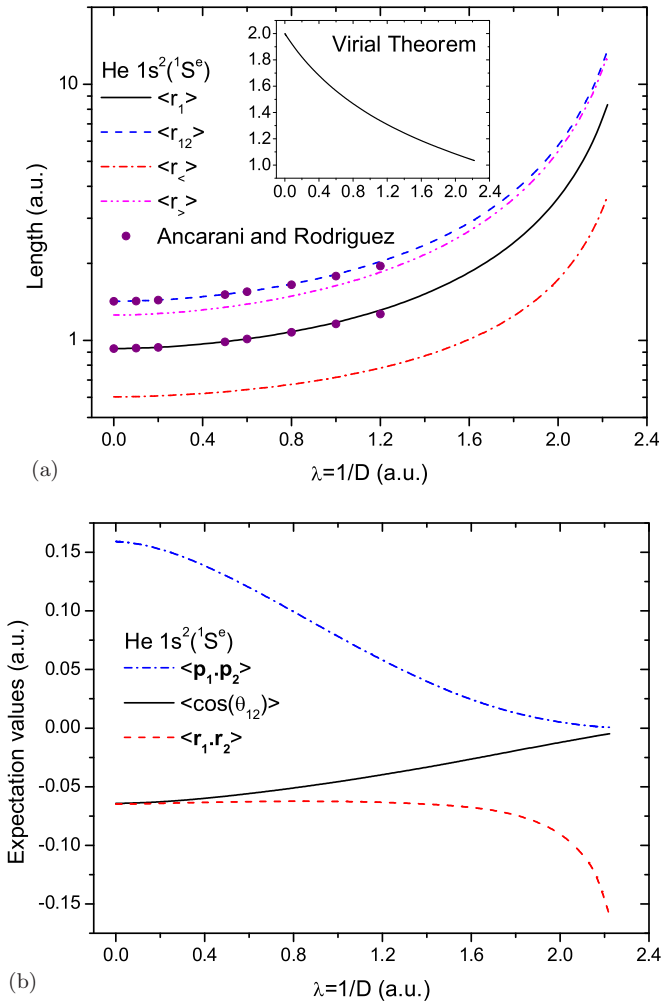

FIG. 3. (Color online) Variation of the expectation values of some physical quantities for the He ground state against the screening parameter λ. (a) $\langle r_1\rangle$, $\langle r_{12}\rangle$, $\langle r_<\rangle$, $\langle r_>\rangle$, and $-\langle V\rangle/\langle T\rangle$; (b) $\langle \mathbf{p_1}\cdot\mathbf{p_2}\rangle$, $\langle\cos(\theta_{12})\rangle$, and $\langle \mathbf{r_1}\cdot\mathbf{r_2}\rangle$. Present results are compared with the calculations of Ancarani and Rodriguez [33] when they are available.

variations of expectation values not only for radial quantities $\langle r_1^n\rangle$, $\langle r_{12}^n\rangle$, $\langle r_<\rangle$, $\langle r_>\rangle$, but also for those including angular correlations $\langle \mathbf{r_1}\cdot\mathbf{r_2}\rangle$, $\langle \mathbf{p_1}\cdot\mathbf{p_2}\rangle$, $\langle\cos(\theta_{12})\rangle$, as well as the virial theorem $-\langle V\rangle/\langle T\rangle$ in the entire screening range where the ground state exists. Comparisons of the present results with the prediction of Ancarani and Rodriguez [33] and other state-of-the-art calculations at $\lambda = 0$ in the literature [62,63] are shown in Fig. 3 and Table IV. The radial scale of He atom increases monotonously when the ground state approaches the bound limit ($E_{\mathrm{He}(1s^2\ ^1S^e)} = E_{\mathrm{He}^+(1s)}$), while the angular correlation quantities show some different trends. The cosine

TABLE III. Energies of the He ($1s^2\ ^1S^e$) ground state and He$^+$($1s$) threshold at different Debye length D. All results are given in atomic units.

D	∞	100	10	5	2	1	0.5	0.45
λ	0	0.01	0.1	0.2	0.5	1	2	2.222 222
He$^+$($1s$)	− 2.000 000	− 1.980 075	− 1.807 266	− 1.628 232	− 1.163 678	− 0.592 468	− 0.041 143	− 0.007 030
Present	− 2.903 68	− 2.873 80	− 2.614 81	− 2.346 96	− 1.655 36	− 0.818 17	− 0.051 74	− 0.008 70
Lin *et al.* [32,58]	− 2.903 58	− 2.873 70	− 2.614 71	− 2.346 86	− 1.655 26	− 0.818 09	− 0.051 72	− 0.008 71
Kar and Ho [29]	− 2.903 724	− 2.873 838	− 2.614 852	− 2.347 006	− 1.655 401	− 0.818 214	− 0.051 69	− 0.008 1
Hashino *et al.* [26]	− 2.903 72	− 2.873 83	− 2.614 85	− 2.347 00		− 0.818 21	− 0.050 34	
Saha *et al.* [25]	− 2.903 716	− 2.873 830			− 1.655 267	− 0.815 999	+0.012 209	
Ancarani *et al.* [33]	− 2.903 37		− 2.614 51	− 2.346 66	− 1.655 04	− 0.817 04		
Lam *et al.* [21]	− 2.902 43	− 2.872 55	− 2.613 50	− 2.345 49	− 1.652 53	− 0.808 51	− 0.006 30	

TABLE IV. Expectation values of some physical quantities for the He ground state ($1s^2\ ^1S^e$) at different Debye length D. All results are given in atomic units.

D	∞		100	10	5	2	1	0.5	0.45
λ	0		0.01	0.1	0.2	0.5	1	2	2.222 222
$\langle r_1^{-1}\rangle$	1.688 317[a]	1.688 31	1.688 27	1.685 01	1.675 78	1.618 28	1.435 43	0.677 99	0.376 80
		1.687 30[b]		1.684 06[b]	1.674 98[b]	1.618 46[b]	1.441 89[b]		
$\langle r_1\rangle$	0.929 472[a]	0.929 47	0.929 50	0.932 18	0.939 74	0.988 46	1.176 03	3.595 43	8.328 62
		0.929 47[b]		0.932 15[b]	0.939 61[b]	0.987 37[b]	1.160 18[b]		
$\langle r_1^2\rangle$	1.193 483[a]	1.193 44	1.193 52	1.201 61	1.224 39	1.375 72	2.047 81	23.865 7	135.609
		1.192 81[b]		1.200 82[b]	1.223 12[b]	1.369 56[b]	1.954 30[b]		
$\langle r_{12}^{-1}\rangle$	0.945 818[a]	0.945 86	0.945 84	0.943 50	0.936 93	0.896 48	0.769 43	0.281 26	0.127 40
		0.946 32[b]		0.943 97[b]	0.937 44[b]	0.897 36[b]	0.775 52[b]		
$\langle r_{12}\rangle$	1.422 070[a]	1.422 08	1.422 13	1.426 26	1.437 95	1.513 73	1.809 79	5.774 61	13.610 7
		1.421 63[b]		1.425 76[b]	1.437 28[b]	1.511 43[b]	1.782 67[b]		
$\langle r_{12}^2\rangle$	2.516 439[a]	2.516 40	2.516 57	2.532 39	2.577 21	2.877 46	4.220 75	47.906 5	271.539
		2.514 72[b]		2.530 43[b]	2.574 41[b]	2.865 78[b]	4.049 53[b]		
$\langle r_<\rangle$	0.602 37[d]	0.602 36	0.602 37	0.603 60	0.607 12	0.630 16	0.717 68	1.728 96	3.662 13
$\langle r_>\rangle$	1.256 66[d]	1.256 58	1.256 63	1.260 76	1.272 36	1.346 77	1.634 38	5.461 91	12.995 1
$\langle \mathbf{r_1}\cdot\mathbf{r_2}\rangle$	−0.064 737[c]	−0.064 76	−0.064 76	−0.064 59	−0.064 22	−0.063 01	−0.062 56	−0.087 58	−0.160 29
$\langle \mathbf{p_1}\cdot\mathbf{p_2}\rangle$	0.159 069[c]	0.159 14	0.159 13	0.157 49	0.153 11	0.129 87	0.078 14	0.004 74	0.000 64
$\langle\cos(\theta_{12})\rangle$	−0.064 27[d]	−0.064 22	−0.064 22	−0.063 87	−0.062 95	−0.058 07	−0.045 78	−0.012 13	−0.004 81
$-\langle V\rangle/\langle T\rangle$	2	2.000 00	1.989 75	1.903 88	1.819 84	1.617 81	1.381 16	1.084 31	1.034 30

[a]Drake [62].
[b]Ancarani and Rodriguez [33].
[c]Grabowski and Chernoff [63].
[d]Lin *et al.* [58].

of the average angle of between two electrons $\langle\cos(\theta_{12})\rangle$ is approaching zero, and the resulting effect for $\langle \mathbf{r_1}\cdot\mathbf{r_2}\rangle$ (negative) is decreasing. Another interesting physical quantity is $\langle \mathbf{p_1}\cdot\mathbf{p_2}\rangle$, which is part of the mass polarization term when finite nuclear mass is considered [see Eq. (1)]. It also reflects the electron correlations in momentum space and its magnitude and sign offer a useful perspective on the relative motion of two electrons [64,65]. The expectation value $\langle \mathbf{p_1}\cdot\mathbf{p_2}\rangle$ decreases to zero with increasing the screening parameter λ. Because the magnitude of electron momentum is always nonzero, even the state is near the bound limit; such a trend indicates a very interesting picture of the evolution of the system in momentum space: The orientations of the two-electron momentums tend to be perpendicular to each other.

It is now clear that the increasing of screening strength would result in the decreasing of electron correlations in both coordinate and momentum spaces. The variations of expectation values of quantities related to angular correlations in ground state show similarities, to some extent, to the situation in singly excited states $1snl$. With successively increasing n, correlations between the two electrons become weaker in both coordinate and momentum spaces and the expectation values of $\langle\cos(\theta_{12})\rangle$ (shown in Table I and compared with Refs. [58,60]) and $\langle \mathbf{p_1}\cdot\mathbf{p_2}\rangle$ (shown in Table I of Ref. [64]) both approach zero.

B. Resonant states

The complex-scaling method is employed to investigate the resonant states of a He atom embedded in screening environment. A two-group CI basis is used in the calculation which includes 12 s-type, 11 p-type, . . . and 1 o-type Slater orbitals with $\xi = 1.0$ in the first group, and 6 s-type, 5 p-type, . . . and 1 h-type orbitals with $\xi = 0.4$ in the second group. The total numbers of basis functions in the expansion of system wave functions are 637 and 998 for the $^1S^e$ and $^1P^o$ states, respectively. For illustrative purpose, we only show the lowest four resonances associated with the $He^+(N = 2, 3,$ and 4) thresholds and emphasis on the capability of the present method. The accuracy of the resonance energy and width calculated by adopting such a basis can be estimated from Table V for resonances at $\lambda = 0$. The brief notation $(N - m)$ represents the mth resonance associated with the $He^+(N)$ threshold. A more physically based classification labeled by approximate quantum numbers ${}_N[K,T]_n^A$ [45,46] is also given for each resonance. The complex-scaling calculations with correlated Sturmian-type basis functions in perimetric coordinates of Bürgers and Lindroth [66] and Rost *et al.* [67] are included as the benchmark. From the comparison, it can be seen that the present results are generally in good agreement with the most accurate ones and the agreement improves further for higher-lying states. The worst prediction of resonance parameters in the CI calculation appears at ${}_2[-1,0]_2^+\ ^1S^e$ state, which is an intrashell resonance having the most negative K value. The two electrons in this state can be located in a close region and the fulfillment of the Kato cusp condition for the basis function is important. Another disadvantage of the present work is the determination of width for the ${}_2[-1,0]_3^+\ ^1P^o$ resonance. An enlarged or correlated basis should be used to produce such an extremely small value. The real parts of expectation values of $\langle\cos(\theta_{12})\rangle$ and $\langle \mathbf{p_1}\cdot\mathbf{p_2}\rangle$ for the resonant states are also shown in Table V. For the $^1S^e$ states, only Krause *et al.* [64] has calculated $\langle \mathbf{p_1}\cdot\mathbf{p_2}\rangle$ for the lowest three resonances. However, our results are significantly

TABLE V. Classifications, energies, widths, and some expectation values for the He doubly excited resonant states in $^1S^e$ and $^1P^o$ symmetries. Only the real parts of $\langle\cos(\theta_{12})\rangle$ and $\langle \mathbf{p_1}\cdot\mathbf{p_2}\rangle$ are given. All the results are given in atomic units.

	$^1S^e$					$^1P^o$				
N-m	${}_N[K,T]^A_n$	E_r	Γ	$\langle\cos(\theta_{12})\rangle$	$\langle \mathbf{p_1}\cdot\mathbf{p_2}\rangle$	${}_N[K,T]^A_n$	E_r	Γ	$\langle\cos(\theta_{12})\rangle$	$\langle \mathbf{p_1}\cdot\mathbf{p_2}\rangle$
(2-1)	${}_2[1,0]^+_2$	−0.777 855	0.004 546	−0.447 47	−0.003 03	${}_2[0,1]^+_2$	−0.693 091	0.001 330	0.032 96	0.015 44
		−0.777 867 6[a]	0.004 541 3[a]				−0.693 134 9[c]	0.001 373 2[c]		
		−0.777 865[b]			−0.000 79[b]		−0.693 13[d]	0.001 38[d]	0.033 12[d]	
(2-2)	${}_2[-1,0]^+_2$	−0.621 82	0.000 15	0.291 17	0.072 53	${}_2[1,0]^-_3$	−0.597 074	0.000 004	−0.416 84	0.0240 7
		−0.621 927 2[a]	0.000 215 6[a]				−0.597 073 8[c]	0.000 003 8[c]		
		−0.621 715[b]			0.077 71[b]		−0.597 073 8[d]	0.000 003 8[d]	−0.416 837[d]	
(2-3)	${}_2[1,0]^+_3$	−0.589 890	0.001 360	−0.483 00	−0.013 62	${}_2[0,1]^+_3$	−0.564 072	0.000 287	0.015 73	0.003 33
		−0.589 894 6[a]	0.001 362 4[a]				−0.564 085 1[c]	0.000 301 1[c]		
		−0.589 96[b]			−0.008 55[b]		−0.564 083 0[d]	0.000 300 2[d]	0.015 690[d]	
(2-4)	${}_2[-1,0]^+_3$	−0.548 067	0.000 061	0.442 31	0.010 67	${}_2[-1,0]^-_3$	−0.547 090	–	0.134 35	0.01108
		−0.548 085 5[a]	0.000 074 7[a]				−0.547 092 7[c]	$\approx 1E-8$[c]		
							−0.547 092 1[d]	$<2E-8$[d]	0.135 95[d]	
(3-1)	${}_3[2,0]^+_3$	−0.353 538	0.003 011	−0.600 80	−0.002 74	${}_3[1,1]^+_3$	−0.335 625	0.007 036	−0.256 45	0.002 86
		−0.353 538 5[a]	0.003 009 8[a]				−0.335 625 9[c]	0.007 023 7[c]		
							−0.335 626[d]	0.007 028[d]	−0.256[d]	
(3-2)	${}_3[0,0]^+_3$	−0.317 467	0.006 663	−0.032 79	0.004 05	${}_3[2,0]^-_4$	−0.285 951	0.000 034	−0.604 26	0.014 77
		−0.317 457 8[a]	0.006 659 8[a]				−0.285 950 7[c]	0.000 034 1[c]		
							−0.285 950 7[d]	0.000 034 1[d]	−0.604 259[d]	
(3-3)	${}_3[2,0]^+_4$	−0.281 072	0.001 502	−0.629 66	−0.012 11	${}_3[-1,1]^+_3$	−0.282 821	0.001 453	0.209 10	0.017 02
		−0.281 072 7[a]	0.001 501 4[a]				−0.282 828 9[c]	0.001 462 0[c]		
							−0.282 826[d]	0.001 462[d]	0.209 14[d]	
(3-4)	${}_3[0,0]^+_4$	−0.263 388	0.002 418	0.032 61	0.007 08	${}_3[1,1]^+_4$	−0.271 193	0.002 901	−0.296 70	−0.002 44
		−0.263 388 3[a]	0.002 418 7[a]				−0.271 193 4[c]	0.002 896 2[c]		
							−0.271 193[d]	0.002 898[d]	−0.296 68[d]	
(4-1)	${}_4[3,0]^+_4$	−0.200 989	0.001 939	−0.690 15	−0.000 51	${}_4[2,1]^+_4$	−0.194 513	0.003 575	−0.412 65	0.001 41
		−0.200 989 5[a]	0.001 938 3[a]				−0.194 512 1[c]	0.003 574 3[c]		
							−0.194 513[d]	0.003 574[d]	−0.412 6[d]	
(4-2)	${}_4[1,0]^+_4$	−0.187 835	0.004 915	−0.200 18	0.003 56	${}_4[0,1]^+_4$	−0.178 799	0.004 770	−0.010 62	0.002 76
		−0.187 834 6[a]	0.004 916 7[a]				−0.178 798 7[c]	0.004 773 1[c]		
							−0.178 80[d]	0.004 78[d]	−0.010 7[d]	
(4-3)	${}_4[-1,0]^+_4$	−0.168 261	0.002 163	0.109 55	0.007 85	${}_4[3,0]^-_5$	−0.168 846	0.000 046	−0.697 45	0.009 80
		−0.168 261 3[a]	0.002 172 3[a]				−0.168 846 0[c]	0.000 046 1[c]		
							−0.168 860 9[d]	0.000 046 0[d]	−0.697 45[d]	
(4-4)	${}_4[3,0]^+_5$	−0.165 734	0.001 210	−0.709 41	−0.008 89	${}_4[2,1]^+_5$	−0.161 252	0.002 168	−0.446 16	−0.003 88
		−0.165 734 0[a]	0.001 210 0[a]				−0.161 251 2[c]	0.002 167 8[c]		
							−0.161 252[d]	0.002 168[d]	−0.446 179[d]	

[a]Bürgers *et al.* [66].
[b]Krause *et al.* [64].
[c]Rost *et al.* [67].
[d]Eiglsperger *et al.* [68].

different from theirs and only the signs of these values can be identified. Eiglsperger *et al.* [68] have calculated $\langle\cos(\theta_{12})\rangle$ for the $^1P^o$ resonances by using a CI basis in Coulomb-Sturmian functions. The agreement between our results and theirs are generally in the same orders of magnitude as that for the energy and width.

The screening effects of SCP on the resonance energy and width have been investigated by Kar and Ho [38–40] using the stabilization method with exponential correlated basis. Accurate resonance parameters have been obtained in a wide range of screening strength, but only for resonances lying below the $He^+(N=2)$ threshold. This may due to the limitation of the stabilization method that the plotted stabilization plateaus become quite complicated for multichannel resonances. Subsequently, the complex-scaling method based on Hylleraas basis functions was applied to calculate the $^1S^e$ resonances associated with the $He^+(N=2$, 3, and 4) thresholds by Chakraborty and Ho [41]. Their results are probably the most accurate predictions of the $^1S^e$ resonance with SCP in the literature up to the present. Most recently, Ordóñez-Lasso *et al.* [44] have presented a systematic study on the $^{1,3}S^e$, $^{1,3}P^o$, and $^{1,3}D^e$ resonances below the $He^+(N=2)$ threshold by using the Feshbach projection method with the Hylleraas basis. The evolutions of resonance energy, width, and average interelectronic angle as a function of screening parameter are investigated for resonances in different series. In Figs. 4 and 5, we compare our results with those previous calculations for resonances in $^1S^e$ and $^1P^o$

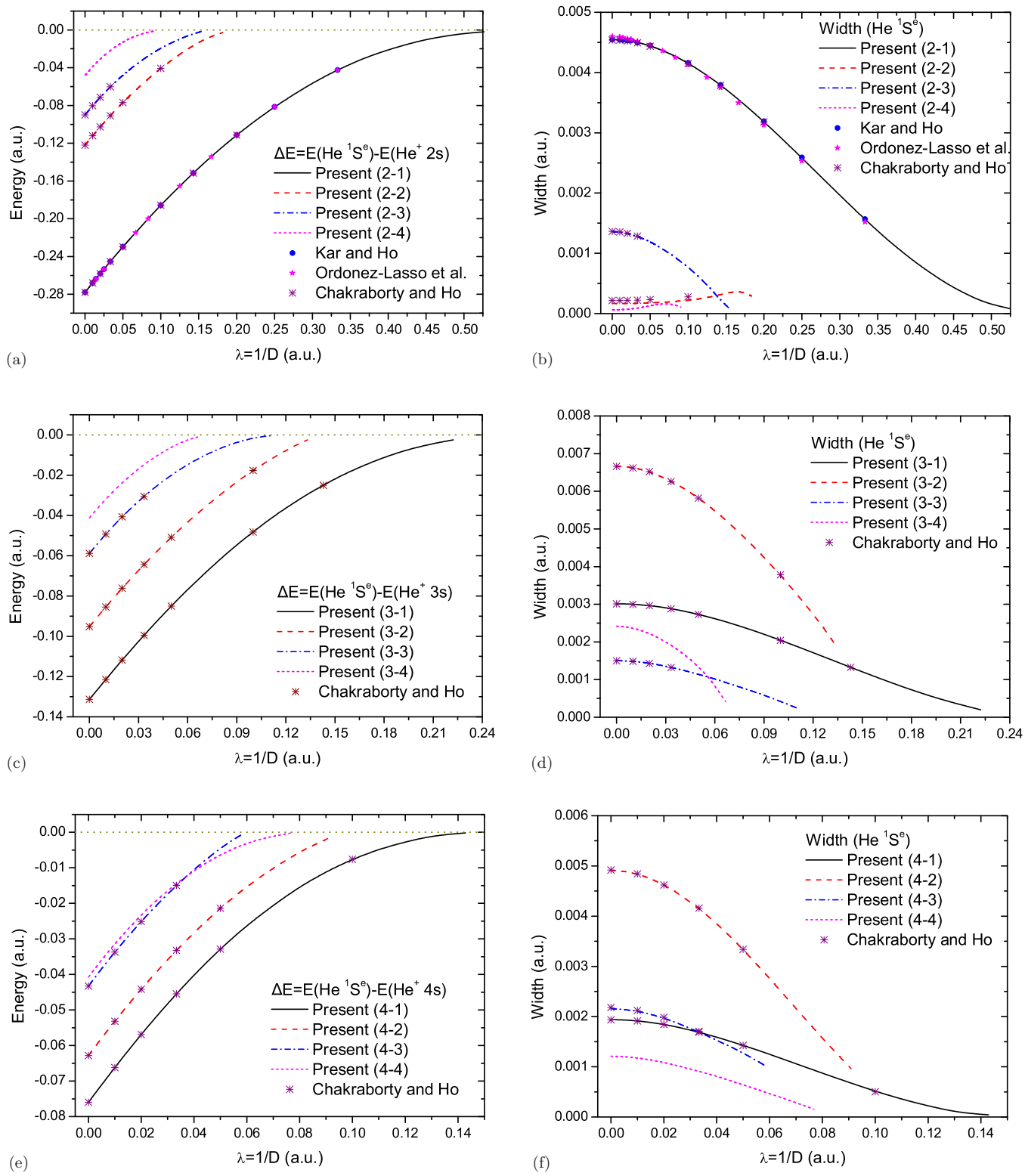

FIG. 4. (Color online) Variation of the energy ($\Delta E = E_{\mathrm{He}} - E_{\mathrm{He}^+(Ns)}$) and width for the He $^1S^e$ resonant states associated with the $\mathrm{He}^+(N = 2\text{–}4)$ thresholds against the screening parameter λ. (a), (b) $N = 2$; (c), (d) $N = 3$; (e), (f), $N = 4$. Present results are compared with the calculations of Kar and Ho [38], Ordóñez-Lasso *et al.* [44], and Chakraborty and Ho [41].

symmetries, respectively. The widths of (2–4) $^1P^o$ resonance are not shown here due to the reasons mentioned above. Numerical values of the lowest $^1S^e$ resonance at some selected values of D are shown in Table VI as an illustration. As we can see, all of the calculations predict similar trends in energy and width for resonances lying below the $\mathrm{He}^+(N = 2)$ threshold. For the $^1S^e$ resonances associated with higher-lying thresholds, our CI calculation gets almost same results as

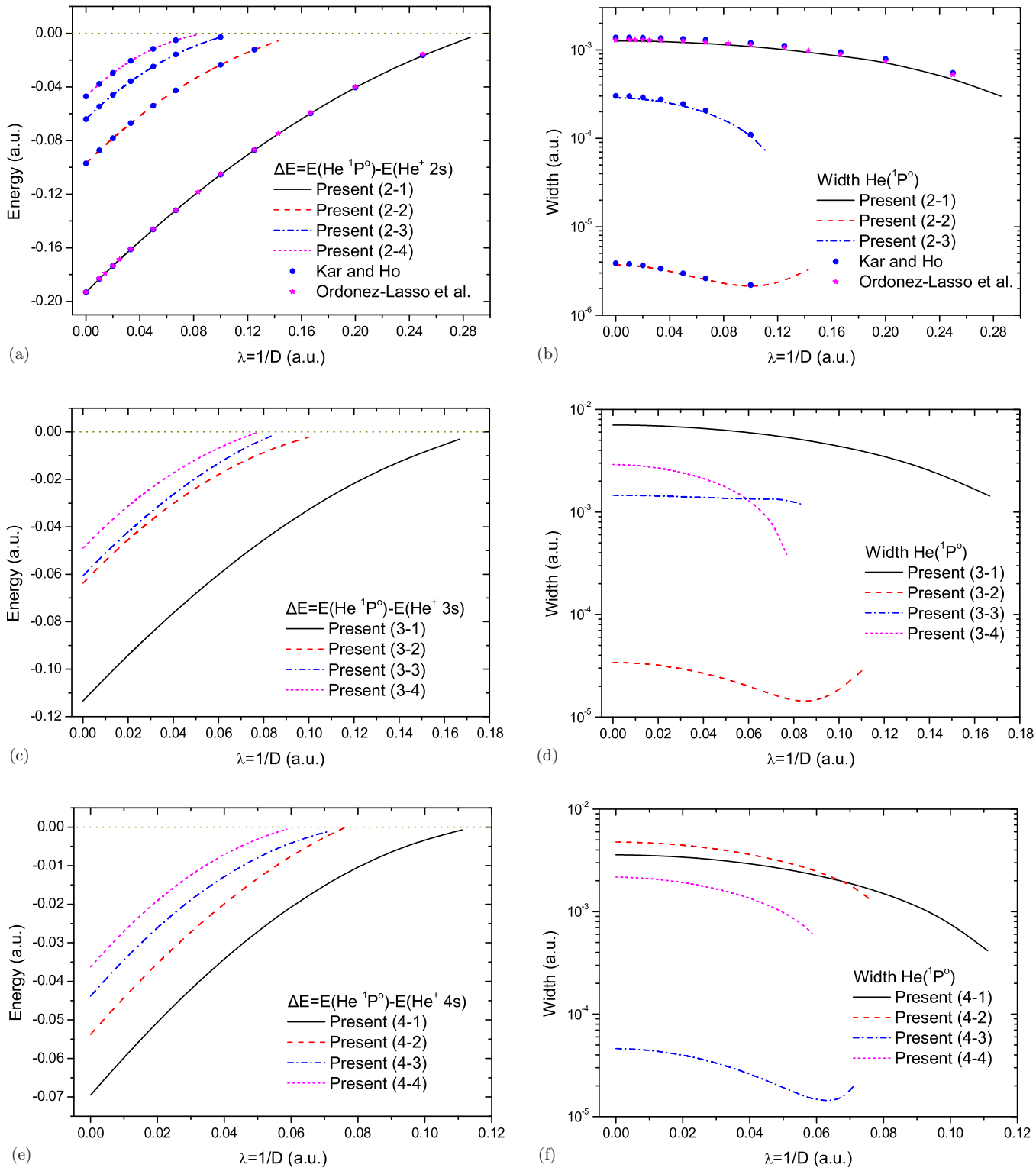

FIG. 5. (Color online) Variation of the energy ($\Delta E = E_{\mathrm{He}} - E_{\mathrm{He}^+(Ns)}$) and width for the He $^1P^o$ resonant states associated with the $\mathrm{He}^+(N = 2\text{–}4)$ thresholds against the screening parameter λ. (a), (b) $N = 2$; (c), (d) $N = 3$; (e), (f) $N = 4$. Present results are compared with the calculations of Kar and Ho [39,40] and Ordóñez-Lasso *et al.* [44].

those obtained by the Hylleraas basis [41]. In Table VI, the systematic behavior of the present calculated resonance parameters is found, like the situation in the ground state (see Table III). The complex-scaling method based on the CI basis show slightly higher energy (0.000 012 a.u.) and wider width (0.000 005 a.u.) than the most accurate results [41] at all screening parameters.

The isomorphic changes of resonance width in a series $_N[K,T]$ against the screening parameter have been demonstrated by Ordóñez-Lasso *et al.* [44] for resonances associated

TABLE VI. Energies and widths for the He $_2[1,0]_2^+$ $^1S^e$ resonant state and bound energies for the $He^+(2s,2p)$ thresholds at different Debye length D. All results are given in atomic units.

D	∞	100	50	20	10	7	5	3
λ	0	0.01	0.02	0.05	0.1	0.142 857	0.2	0.333 333
$He^+(2s)$	− 0.500 000	− 0.480 297	− 0.461 173	− 0.407 104	− 0.327 085	− 0.267 535	− 0.199 713	− 0.085 619
$He^+(2p)$	− 0.500 000	− 0.480 248	− 0.460 981	− 0.405 970	− 0.322 962	− 0.259 782	− 0.186 138	− 0.057 934
E_r								
Present	− 0.777 855	− 0.748 223	− 0.719 320	− 0.636 844	− 0.512 818	− 0.419 094	− 0.311 064	− 0.127 938
Chakraborty and Ho [41]	− 0.777 867	− 0.748 236	− 0.719 333	− 0.636 856	− 0.512 829	− 0.419 105	− 0.311 073	
Kar and Ho [40]	− 0.777 83	− 0.748 19	− 0.719 29	− 0.636 83	− 0.512 79	− 0.419 06	− 0.311 05	− 0.127 92
Ordóñez-Lasso *et al.* [44]	− 0.777 94	− 0.748 31	− 0.719 41	− 0.636 94	− 0.512 91	− 0.419 19	− 0.311 14	− 0.127 98
Γ								
Present	0.004 546	0.004 542	0.004 529	0.004 441	0.004 153	0.003 790	0.003 185	0.001 564
Chakraborty and Ho [41]	0.004 541	0.004 537	0.004 524	0.004 436	0.004 149	0.003 786	0.003 181	
Kar and Ho [40]	0.004 549	0.004 545	0.004 533	0.004 450	0.004 159	0.003 794	0.003 191	0.001 569
Ordóñez-Lasso *et al.* [44]	0.004 60	0.004 59	0.004 56	0.004 45	0.004 13	0.003 75	0.003 13	0.001 52

with the $He^+(N = 2)$ threshold. Furthermore, as one can see from Fig. 5, the isomorphism also exists among resonances in different shells, for example, the (2-2) $_2[1,0]_3^-$, (3-2) $_3[2,0]_4^-$, and (4-3) $_4[3,0]_5^-$ $^1P^o$ resonances shown in Figs. 5(b), 5(d), and 5(f), respectively. This phenomenon can be understood from the molecular picture originated by Herrick and Kellman [45,69] that the doubly excited resonant states can be interpreted in terms of the collective ro-vibrational motions of a highly nonrigid X-Y-X molecule, with the X's electrons and Y the nucleus. The bending vibrational quanta of the resonant states is defined by $\nu = N$-K-1 and the rotational angular momentum along the molecule-fixed axis (internal axis of the two-electron atoms) is given by the approximate quantum number T. All the three resonances associated with different thresholds mentioned above have zero bending quanta and zero rotational angular momentum along the internal axis. Therefore, their widths are in the same order of magnitude and follow a similar behavior in changing the screening parameter.

The investigations on physical quantities other than energy and width would yield more information in understanding the evolution of resonant states in screening environment. Such work is available by Ordóñez-Lasso *et al.* [44], who have presented a detailed study on the interelectronic angle $\arccos\langle\cos(\theta_{12})\rangle$ for He resonances at different screening parameters. In their calculation, all the angles would ultimately approach 90° with increasing λ to the critical point beyond which the resonances will be no longer exist. In Figs. 6(a) and 6(b), we compare our results calculated by using the complex-scaled CI wave functions with those of Ordóñez-Lasso *et al.* [44] for the lowest six $^1P^o$ resonances associated with the $He^+(N = 2)$ threshold. It is interestingly found that the interelectronic angles of (2-1), (2-3), and (2-6) resonances in Fig. 6(a) belonging to $_2[0,1]^+$ series are moving away from 90° with increasing λ, which is opposite to the prediction of Ordóñez-Lasso *et al.* [44]. Although the general trends for the (2-2), (2-4), and (2-5) resonances in Fig. 6(b) are the same in both calculations, the results are quantitatively different. Recalling that our results are in good agreement with the prediction of Eiglsperger *et al.* [68] at $\lambda = 0$, we have also performed a calculation by using the Feshbach projection method [70] with the B-spline CI basis [32,58] for further examination. It is clearly shown that our two individual methods based on different basis sets get almost same results at all λ investigated here which, further assures the reliability of the present results. Recalling the changes of interelectronic angle in the bound states—that they are all approaching 90° when the states are close to the bound limits—the angles in the resonant states may have different behaviors due to their asymptotically divergent wave functions in different configurations. Due to the fact that the $He^+(2s)$ and $(2p)$ states are not degenerate in the screening environment and some of the resonant states would exceed the $He^+(2s)$ threshold and transform into resonances owing shape characters, the critical points for the existence of these resonances are not asserted in this work. Another interesting phenomenon is that the interelectronic angles of (2-4) and (2-5) resonances displayed in Fig. 6(b) show a strong interference effect at small values of λ. We present a tentative explanation that this is due to the near-degenerate energies for these two resonances. As shown in the embedded figure, the (2-4) and (2-5) resonances have much closer energies than others at small λ. When λ increases to larger values, the two resonances are well separated and the interference effect becomes weaker. At present, it is still unknown that how the near-degenerate resonances affect each other in the screening environment.

The results for resonances associated with $He^+(N = 3$ and 4) thresholds are shown in Figs. 6(c) and 6(d), respectively. These relatively lower-lying resonances associated with a certain threshold approach 90°, except the (4-2) resonance, which exceeds 90° to smaller angles. Similarly, such phenomenon may be due to the near-degenerate energies between the (4-2) and (4-3) resonances at $\lambda = 0.06$–0.08. The interference effects in relatively higher-lying resonances associated with a specified or different thresholds are expected to be more complicated due to the close proximity of large numbers of resonances in the energy range near the thresholds.

Besides $\langle\cos(\theta_{12})\rangle$, we have also calculated $\langle\mathbf{p_1}\cdot\mathbf{p_2}\rangle$ for the $^1P^o$ resonances investigated here and the results are shown in Fig. 7. No comparisons can be made at present even in the pure Coulomb case. From Fig. 7(a) we can see that the interference effect existing between the interelectronic angles of (2-4) and

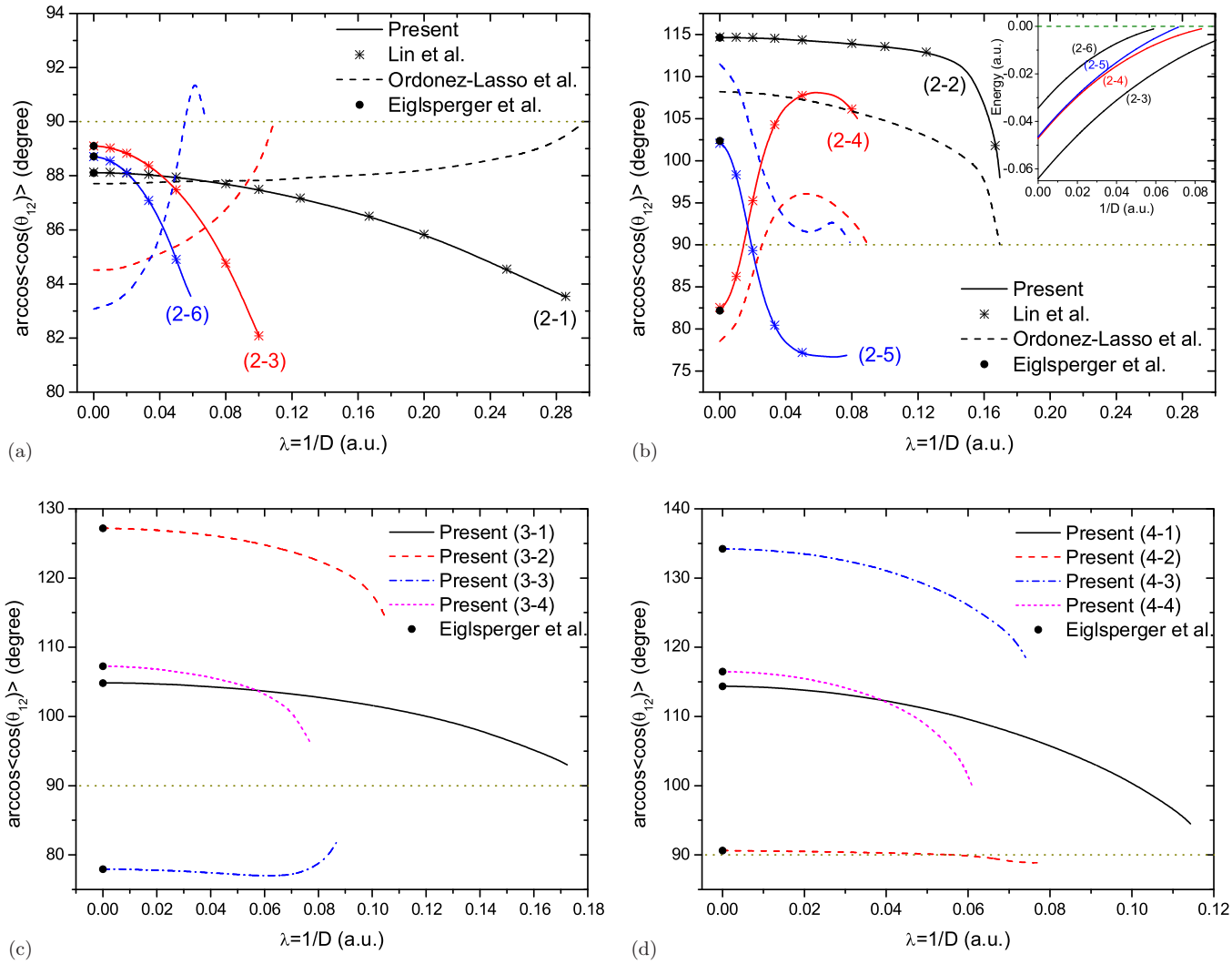

FIG. 6. (Color online) Variation of $\arccos\langle\cos(\theta_{12})\rangle$ for the He $^1P^o$ resonant states associated with the $He^+(N = 2–4)$ thresholds against the screening parameter λ. (a), (b) $N = 2$; (c) $N = 3$; (d) $N = 4$. Present results are compared with the calculations of Lin *et al.* [58], Ordóñez-Lasso *et al.* [44], and Eiglsperger *et al.* [68].

(2-5) resonances are also visible in $\langle \mathbf{p_1} \cdot \mathbf{p_2} \rangle$, although in a relatively small magnitude. The most interesting phenomenon in the variation of $\langle \mathbf{p_1} \cdot \mathbf{p_2} \rangle$ against the screening parameter is that the lowest resonance associated with $He^+(N = 2$ and 3) thresholds and the lowest two with the $He^+(N = 4)$ threshold have the positive expectation values first decreasing and then slightly increasing, whereas the rest of others have values approaching zero. With further examination on these resonances one can find they are all intrashell resonances with positive values of K and, consequently, can be more likely interpreted as a symmetric, linearly moving X-Y-X molecule in view of the picture of Herrick and Kellman [45,69]. Because the magnitude of momentum (i.e., $\langle \mathbf{p_1}^2 \rangle = \langle 2\mu T_1 \rangle$) for each electron is always decreasing with increasing λ, we can only deduce that the movement of the two electrons in these states are increasingly synchronous in a same direction. Analyzing the absolute magnitude of $\langle \mathbf{p_1} \cdot \mathbf{p_2} \rangle$ is difficult because it contains both radial and angular correlations in momentum space. Further investigations on other quantities, such as $\langle p_{12} \rangle = \langle |\mathbf{p_1} - \mathbf{p_2}| \rangle$, describing the magnitude of relative momentum between two electrons [71], $\langle \cos(\bar{\theta}_{12}) \rangle$ the angle subtended between two momentum vectors of electrons [72], and $\rho(p_1, p_2)$ the density of system wave function in momentum space [73], will be welcomed in the future to shed more light on the evolution of resonant states in screening environment.

IV. CONCLUSIONS

In this work, we have applied the variational and complex-scaling methods together with the Slater-type CI basis functions to investigate the bound and resonant states of two-electron systems embedded in screening environment. Two expansion methods, Taylor expansion and Gegenbauer expansion, are introduced to analytically deal with the two-electron SCP matrices in both the real and complex formalism. The former has great advantages in fast computation of the matrix elements at small screening parameters, while the latter is applicable in arbitrary screening conditions. Convergences of Taylor expansion at different λ are examined. The computations of expectation values for different physical quantities

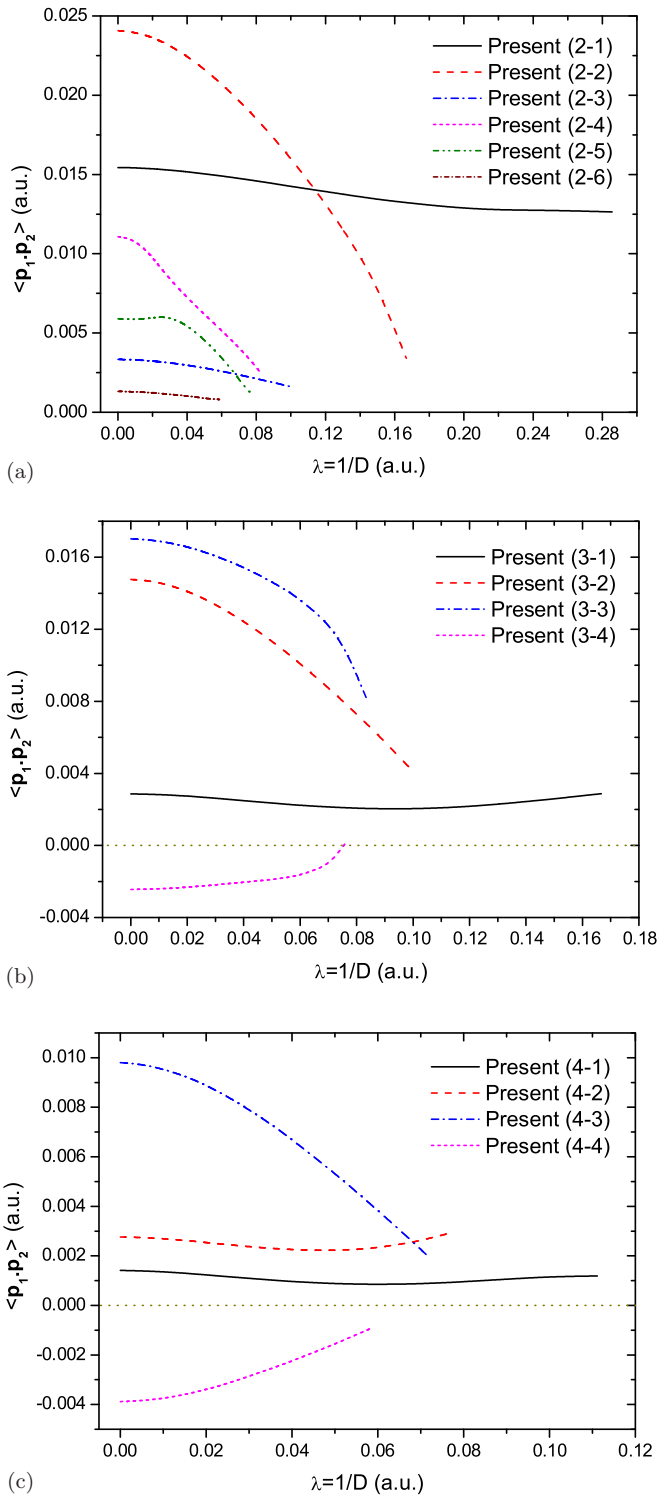

FIG. 7. (Color online) Variation of $\langle \mathbf{p_1} \cdot \mathbf{p_2} \rangle$ for the He $^1P^o$ resonant states associated with the $He^+(N = 2\text{–}4)$ thresholds against the screening parameter λ. (a) $N = 2$; (b) $N = 3$; (c) $N = 4$.

by using the complex-scaled resonance wave function are introduced.

Variations of the bound-state energies for He ground and several singly excited states in $^1S^e$ and $^1P^o$ symmetries are investigated. Our results are in systematic agreement with previous accurate predictions by using correlated basis functions. For the ground states, the evolutions of physical quantities such as $\langle r_1^n \rangle$, $\langle r_{12}^n \rangle$, $\langle r_< \rangle$, $\langle r_< \rangle$, $\langle \mathbf{r_1} \cdot \mathbf{r_2} \rangle$, $\langle \mathbf{p_1} \cdot \mathbf{p_2} \rangle$, $\langle \cos(\theta_{12}) \rangle$, and $-\langle V \rangle / \langle T \rangle$ are calculated in the entire screening range where the ground state exists. The accuracy of these results is expected to be in the same degree as that in the pure Coulomb situation.

The doubly excited resonant states of the He atom associated with the $He^+(N = 2, 3, \text{and } 4)$ thresholds are calculated by using the complex-scaling method at different screening parameters. The energy and width are in good agreement with other theoretical calculations when they are available, whereas the average interelectronic angles $\arccos\langle \cos(\theta_{12}) \rangle$ are quite different from those by the Feshbach projection method with the Hylleraas basis. The accuracy of the present work is ensured by performing an independent Feshbach projection calculation with the B-spline CI basis. The behaviors of the interelectronic angle for resonant states in a screening environment are found to be different from those for bound states due to their asymptotically divergent wave functions and complicated configuration interactions. Strong interference effects exist between resonances with near-degenerate energies. Additionally, we have calculated the quantity $\langle \mathbf{p_1} \cdot \mathbf{p_2} \rangle$ for the resonant states as a function of λ. Its variation may partially reflects the electron correlations of resonant states on momentum properties.

The computational methods introduced in this work can be fairly applied to the two-electron systems with arbitrary nuclear charge and mass (e.g., H^-, Ps^-, and Li^+) confined in generalized-form SCPs, such as the exponential-cosine SCP [74–77] and the finite oscillator potential [78,79]. The former has been widely used to describe the multiparticle cooperative effects in dense quantum plasmas, while the latter has important applications in modeling the Coulomb interactions of charged particles confined in quantum dots.

Finally, we would like to emphasize that, although the present work is applicable to the two-electron atoms embedded in plasmas modeled by SCP, both the experimental observations and the theoretical predictions of the bound states, resonances, and spectra properties of atoms in a real plasma are more complicated than those in vacuum space. Experimental measurement requires not only the production of a weakly coupled plasma environment, but also the precise control of the plasma parameters, such as Debye length, plasma temperature, and number density. For the theoretical side, finding proper model potentials to describe the screening effects between different species and accurately solving the Hamiltonian of such a system are necessary. In fact, there are many elementary processes in a real plasma, such as the radiative transitions, collisional excitations and ionizations, autoionization, as well as the microscopic electric field created by fluctuations. So many processes can occur that the experimental identification of those processes in a particular situation is a major challenge [80]. However, once such identification can be made, the energies of the atomic states can be directly measured from the radiative transition spectra, and the resonance structures can be viewed from the electron-ion scattering cross sections or photoionization cross sections. On the other hand, the theoretical reference data can be used as the diagnostic tool to determine the plasma parameters, especially the Debye length, which, in turn, would lead to estimation of the temperature and

number density of the plasma. With continuous development in both experimental techniques and theoretical investigations, it is believed that the measurement of individual atomic process in plasmas and the theoretical calculations in a more realistic plasma environment will be available in the future.

ACKNOWLEDGMENTS

Financial support by the Ministry of Science and Technology of Taiwan (R.O.C.) is gratefully acknowledged.

APPENDIX

For convenience, we use the same notations used in Ref. [15], i.e.,

$$R_{\triangle}^{L+\frac{1}{2}}(i,j,k,l) = I_{L+\frac{1}{2}}^{n,n'}(\lambda,\xi,\xi'), \tag{A1}$$

where

$$\begin{aligned} n &= n_i + n_k - L - 1, \quad \xi = \xi_i + \xi_k, \\ n' &= n_j + n_l - L - 1, \quad \xi' = \xi_j + \xi_l. \end{aligned} \tag{A2}$$

The general idea to get the analytical solution of this integration is to integrate the inner part of $K(z)$ and the outer part of $I(z)$, one after another. We first calculate the inner integral

$$\rho_{L+\frac{1}{2}} = \int_{r'}^{\infty} dr\left[r^{n+L+\frac{1}{2}} e^{-\xi r} K_{L+\frac{1}{2}}(\lambda r)\right]. \tag{A3}$$

By substituting the exact formula of $K(z)$,

$$K_{n+\frac{1}{2}}(z) = \sqrt{\frac{\pi}{2z}} e^{-z} \sum_{k=0}^{n} \frac{(n+k)!}{k!(n-k)!(2z)^k}, \tag{A4}$$

into Eq. (A3) and using the definition of the incomplete Γ function

$$\Gamma(n,x) = \int_x^{\infty} t^{n-1} e^{-t} dt, \tag{A5}$$

one has

$$\begin{aligned} \rho_{L+\frac{1}{2}} &= \frac{\sqrt{\pi}}{(2\lambda)^{L+\frac{1}{2}}} \sum_{k=0}^{L} \frac{(2L-k)!(2\lambda)^k}{(L-k)!k!} \frac{1}{(\xi+\lambda)^{n+k+1}} \\ &\quad \times \Gamma[(n+k+1),(\xi+\lambda)r'] \\ &= \frac{\sqrt{\pi} e^{-(\xi+\lambda)r'}}{(2\lambda)^{L+\frac{1}{2}}(\xi+\lambda)^{n+1}} \left\{ \sum_{i=0}^{n} \frac{[(\xi+\lambda)r']^i}{i!} Q_0^{Ln}\left(\frac{2\lambda}{\xi+\lambda}\right) \right. \\ &\quad \left. + (1-\delta_{L0}) \sum_{i=1}^{L} \frac{[(\xi+\lambda)r']^{n+i}}{(n+i)!} Q_i^{Ln}\left(\frac{2\lambda}{\xi+\lambda}\right) \right\}, \end{aligned} \tag{A6}$$

where

$$Q_i^{Ln}(z) = \sum_{k=i}^{L} \frac{(2L-k)!(n+k)!}{(L-k)!} \frac{z^k}{k!}, \quad 0 \leqslant i \leqslant L. \tag{A7}$$

The result of $\rho_{L+\frac{1}{2}}$ is the same as Eq. (40) in Ref. [15] except that an additional minus appears in the latter, which we believe should be removed.

In the next step of calculating the outer integral,

$$\tau_{L+\frac{1}{2}}^{m} = \frac{\sqrt{\pi}}{(2\lambda)^{L+\frac{1}{2}}} \int_0^{\infty} dr\left[r^{m+L+\frac{1}{2}} e^{-(\xi+\xi'+\lambda)r} I_{L+\frac{1}{2}}(\lambda r)\right], \tag{A8}$$

we make a transformation

$$I_\nu(z) = i^{-\nu} J_\nu(iz), \tag{A9}$$

where $J(z)$ is the Bessel function of the first kind. Equation (A8) now becomes

$$\begin{aligned} \tau_{L+\frac{1}{2}}^{m} &= \frac{\sqrt{\pi}}{(2\lambda)^{L+\frac{1}{2}}} i^{-(L+\frac{1}{2})} \\ &\quad \times \int_0^{\infty} dr\left[r^{m+L+\frac{1}{2}} e^{-(\xi+\xi'+\lambda)r} J_{L+\frac{1}{2}}(i\lambda r)\right]. \end{aligned} \tag{A10}$$

By using the definite integral

$$\begin{aligned} &\int_0^{\infty} dx[x^{\mu-1} e^{-\alpha x} J_\nu(\beta x)] \\ &= \frac{\left(\frac{\beta}{2\alpha}\right)^\nu \Gamma(\nu+\mu)}{\alpha^\mu \Gamma(\nu+1)} {}_2F_1 \\ &\quad \times \left(\frac{\nu+\mu}{2}, \frac{\nu+\mu+1}{2}; \nu+1; -\frac{\beta^2}{\alpha^2}\right) \end{aligned} \tag{A11}$$

and making the substitutions

$$\begin{aligned} \alpha &= \xi + \xi' + \lambda, \quad \beta = i\lambda, \\ \mu &= L + m + \tfrac{3}{2}, \quad \nu = L + \tfrac{1}{2}, \end{aligned} \tag{A12}$$

we have

$$\begin{aligned} \tau_{L+\frac{1}{2}}^{m} &= \frac{\sqrt{\pi}}{(2)^{2L+1}} \frac{1}{(\xi+\xi'+\lambda)^{2L+2+m}} \frac{\Gamma(2L+2+m)}{\Gamma\left(L+\frac{3}{2}\right)} {}_2F_1 \\ &\quad \times \left[L+1+\frac{m}{2}, L+\frac{3}{2}+\frac{m}{2}; L+\frac{3}{2}; \frac{\lambda^2}{(\xi+\xi'+\lambda)^2}\right] \\ &= \frac{(\xi+\xi'+\lambda)^m}{[(\xi+\xi')(\xi+\xi'+2\lambda)]^{L+m+1}} \frac{(2L+1+m)!L!}{(2L+1)!} {}_2F_1 \\ &\quad \times \left[-\frac{m}{2}, \frac{1-m}{2}; L+\frac{3}{2}; \frac{\lambda^2}{(\xi+\xi'+\lambda)^2}\right], \end{aligned} \tag{A13}$$

with a restriction of $n \leqslant m \leqslant n + n' + L$, where ${}_2F_1(a,b;c;z)$ is the Gauss hypergeometric function.

It is interesting to note that one of the first two variables of the hypergeometric function is always a negative integer. In this case, the infinite summation of the hypergeometric function becomes a finite one,

$${}_2F_1(-m,b;c;z) = \sum_{n=0}^{m} \frac{(-m)_n (b)_n}{(c)_n} \frac{z^n}{n!}, \quad |z| \leqslant 1, \tag{A14}$$

where

$$(x)_n = 1 \cdot x \cdots (x+n-1), \text{ and } (x)_0 = 1. \tag{A15}$$

The result of $\tau^{m}_{L+\frac{1}{2}}$ obtained in Ref. [15] can simply be reproduced by using a transformation of the Gauss hypergeometric function [54].

Combining Eqs. (A6) and (A13), the final expression for the two-dimensional integral of (A1) is given by

$$I^{n,n'}_{L+\frac{1}{2}}(\lambda,\xi,\xi') = \frac{1}{(\xi'+\lambda)^{n'+1}} Q_0^{Ln'}\left(\frac{2\lambda}{\xi'+\lambda}\right)\sum_{i=0}^{n'}\frac{(\xi'+\lambda)^i}{i!}\tau^{n+i}_{L+\frac{1}{2}} + \frac{(1-\delta_{L0})}{(\xi'+\lambda)^{n'+1}}\sum_{i=0}^{L}\frac{(\xi'+\lambda)^{n'+i}}{(n'+i)!}Q_i^{Ln'}\left(\frac{2\lambda}{\xi'+\lambda}\right)\tau^{n+n'+i}_{L+\frac{1}{2}}, \quad \text{(A16)}$$

which is the same as Eq. (10) in Ref. [15], except that a factor $(\xi'+\lambda)^{-(n'+1)}$ was missed in their second term on the right-hand side.

[1] Y. D. Jung, Phys. Plasmas **5**, 3781 (1998).
[2] S. Kar and Y. K. Ho, New J. Phys. **7**, 141 (2005).
[3] F. Pont and P. Serra, Phys. Rev. A **79**, 032508 (2009).
[4] A. N. Sil, S. Canutob, and P. K. Mukherjee, Adv. Quantum Chem. **58**, 115 (2009).
[5] S. B. Zhang, J. G. Wang, and R. K. Janev, Phys. Rev. Lett. **104**, 023203 (2010).
[6] I. Nagy, Phys. Rev. A **83**, 044503 (2011).
[7] P. K. Mondal, N. N. Dutta, G. Dixit, and S. Majumder, Phys. Rev. A **87**, 062502 (2013).
[8] J. Carbonell, F. de Soto, and V. A. Karmanov, Few-Body Syst. **54**, 2255 (2013).
[9] M. Shi, Q. Liu, Z. M. Niu, and J. Y. Guo, Few-Body Syst. **55**, 135 (2014).
[10] Y. D. Kwon, Phys. Rev. B **73**, 165210 (2006).
[11] M. Genkin and E. Lindroth, Phys. Rev. B **81**, 125315 (2010).
[12] Y. Akinaga and S. Ten-no, Chem. Phys. Lett. **462**, 348 (2008).
[13] Y. Akinaga and S. Ten-no, Int. J. Quantum Chem. **109**, 1905 (2009).
[14] M. Seth and T. Ziegler, J. Chem. Theory Comput. **8**, 901 (2012).
[15] J. F. Rico, R. López, G. Ramírez, and I. Ema, Theor. Chem. Acc. **132**, 1304 (2013).
[16] F. J. Rogers, H. C. Graboske, and D. J. Harwood, Phys. Rev. A **1**, 1577 (1970).
[17] C. S. Lam and Y. P. Varshni, Phys. Rev. A **4**, 1875 (1971).
[18] K. M. Roussel and R. F. O'Connell, Phys. Rev. A **9**, 52 (1974).
[19] R. L. Greene and C. Aldrich, Phys. Rev. A **14**, 2363 (1976).
[20] B. Saha, P. K. Mukherjee, and G. H. F. Diercksen, Astron. Astrophys. **396**, 337 (2002).
[21] C. S. Lam and Y. P. Varshni, Phys. Rev. A **27**, 418 (1983).
[22] Z. Wang and P. Winkler, Phys. Rev. A **52**, 216 (1995).
[23] P. K. Mukherjee, J. Karwowski, and G. H. F. Diercksen, Chem. Phys. Lett. **363**, 323 (2002).
[24] S. T. Dai, A. Solovyova, and P. Winkler, Phys. Rev. E **64**, 016408 (2001).
[25] B. Saha, T. K. Mukherjee, P. K. Mukherjee, and G. H. F. Diercksen, Theor. Chem. Acc. **108**, 305 (2002).
[26] T. Hashino, S. Nakazaki, T. Kato, and H. Kashiwabara, Phys. Lett. A **123**, 236 (1987).
[27] S. Dutta, J. K. Saha, S. Bhattacharyya, P. K. Mukherjee, and T. K. Mukherjee, Phys. Scr. **89**, 015401 (2014).
[28] S. Kar and Y. K. Ho, Phys. Rev. A **71**, 052503 (2005).
[29] S. Kar and Y. K. Ho, Int. J. Quantum Chem. **106**, 814 (2006).
[30] S. Kar and Y. K. Ho, Int. J. Quantum Chem. **107**, 353 (2007).
[31] P. Serra and S. Kais, J. Phys. B: At. Mol. Opt. Phys. **45**, 235003 (2012).
[32] Y. C. Lin, C. Y. Lin, and Y. K. Ho, Phys. Rev. A **85**, 042516 (2012).
[33] L. U. Ancarani and K. V. Rodriguez, Phys. Rev. A **89**, 012507 (2014).
[34] A. Basu, J. Phys. B: At. Mol. Opt. Phys. **43**, 115202 (2010).
[35] A. Basu, Eur. Phys. J. D **65**, 405 (2011).
[36] S. B. Zhang, J. G. Wang, and R. K. Janev, Phys. Rev. A **81**, 032707 (2010).
[37] S. B. Zhang, J. G. Wang, R. K. Janev, and X. J. Chen, Phys. Rev. A **83**, 032724 (2011).
[38] S. Kar and Y. K. Ho, Chem. Phys. Lett. **402**, 544 (2005).
[39] S. Kar and Y. K. Ho, Phys. Rev. A **72**, 010703 (2005).
[40] S. Kar and Y. K. Ho, J. Phys. B: At. Mol. Opt. Phys. **39**, 2445 (2006).
[41] S. Chakraborty and Y. K. Ho, Eur. Phys. J. D **49**, 59 (2008).
[42] L. G. Jiao and Y. K. Ho, Int. J. Quantum Chem. **113**, 2569 (2013).
[43] L. G. Jiao and Y. K. Ho, Phys. Rev. A **87**, 052508 (2013).
[44] A. F. Ordóñez-Lasso, J. C. Cardona, and J. L. Sanz-Vicario, Phys. Rev. A **88**, 012702 (2013).
[45] D. R. Herrick, Adv. Chem. Phys. **52**, 1 (1983).
[46] C. D. Lin, Phys. Rev. Lett. **51**, 1348 (1983).
[47] W. P. Reinhardt, Annu. Rev. Phys. Chem. **33**, 223 (1982).
[48] Y. K. Ho, Phys. Rep. **99**, 1 (1983).
[49] N. Moiseyev, Phys. Rep. **302**, 212 (1998).
[50] T. Kato, Commun. Pure Appl. Math. **10**, 151 (1957).
[51] P. Winkler, Int. J. Quantum Chem. **110**, 3129 (2010).
[52] O. Čertík and P. Winkler, Int. J. Quantum Chem. **113**, 2012 (2013).
[53] J. F. Perkins, J. Chem. Phys. **48**, 1985 (1968).
[54] I. S. Gradshteyn and I. M. Ryzhik, in *Table of Integrals, Series, and Products*, 6th ed., edited by A. Jeffrey and D. Zwillinger (Academic Press, New York, 2000).
[55] A. Buchleitner, B. Gremaud, and D. Delande, J. Phys. B: At. Mol. Opt. Phys. **27**, 2663 (1994).
[56] A. Bürgers and J. M. Rost, J. Phys. B: At. Mol. Opt. Phys. **29**, 3825 (1996).
[57] C. F. Fischer, T. Brage, and P. Jönsson, *Computational Atomic Structure* (Institute of Physics, Bristol, Philadelphia, 1997).
[58] Y. C. Lin, C. Y. Lin, and Y. K. Ho (unpublished).
[59] G. W. F. Drake and Z. C. Yan, Chem. Phys. Lett. **229**, 486 (1994).
[60] T. Koga, H. Matsuyama, and A. J. Thakkar, Chem. Phys. Lett. **512**, 287 (2011).
[61] G. W. F. Drake and Z. C. Yan, Phys. Rev. A **46**, 2378 (1992).
[62] G. W. F. Drake, in *Atomic, Molecular, and Optical Physics Handbook*, edited by G. W. F. Drake (AIP, New York, 1996), Vol. 11.

[63] P. E. Grabowski and D. F. Chernoff, Phys. Rev. A **84**, 042505 (2011).
[64] J. L. Krause, J. D. Morgan, and R. S. Berry, Phys. Rev. A **35**, 3189 (1987).
[65] J. W. Hollett and P. M. W. Gill, J. Chem. Theory Comput. **8**, 1657 (2012).
[66] A. Bürgers, D. Wintgen, and J. M. Rost, J. Phys. B: At. Mol. Opt. Phys. **28**, 3163 (1995).
[67] J. M. Rost, K. Schulz, M. Domke, and G. Kaindl, J. Phys. B: At. Mol. Opt. Phys. **30**, 4663 (1997).
[68] J. Eiglsperger, M. Schönwetter, B. Piraux, and J. M. Nero, At. Data Nucl. Data Tables **98**, 120 (2012).
[69] M. E. Kellman and D. R. Herrick, Phys. Rev. A **22**, 1536 (1980).
[70] A. Temkin, in *Atomic, Molecular, and Optical Physics Handbook*, edited by G. W. F. Drake (AIP, New York, 1996), Vol. 25.
[71] D. R. T. Keeble and K. E. Banyard, J. Phys. B: At. Mol. Opt. Phys. **30**, 13 (1997).
[72] T. Koga and H. Matsuyama, Chem. Phys. Lett. **375**, 565 (2003).
[73] B. Talukdar, A. Sarkar, S. N. Roy, and P. Sarkar, Chem. Phys. Lett. **381**, 67 (2003).
[74] D. Singh and Y. P. Varshni, Phys. Rev. A **28**, 2606 (1983).
[75] A. Ghoshal and Y. K. Ho, Phys. Rev. A **79**, 062514 (2009).
[76] A. K. Roy, Int. J. Quantum Chem. **113**, 1503 (2013).
[77] A. Bhattacharya, M. Z. M. Kamali, A. Ghoshal, and K. Ratnavelu, Phys. Plasmas **20**, 083514 (2013).
[78] P. Kimani, P. Jones, and P. Winkler, Int. J. Quantum Chem. **108**, 2763 (2008).
[79] S. Chakraborty and Y. K. Ho, Phys. Rev. A **84**, 032515 (2011).
[80] J. Weisheit, in *Atomic, Molecular, and Optical Physics Handbook*, edited by G. W. F. Drake (AIP, New York, 1996), Vol. 82.